



## Towards Neuro-Fuzzy Compensated PID Control of Lower Extremity Exoskeleton System for Passive Gait Rehabilitation

Jyotindra Narayan & Santosha Kumar Dwivedy

To cite this article: Jyotindra Narayan & Santosha Kumar Dwivedy (2020): Towards Neuro-Fuzzy Compensated PID Control of Lower Extremity Exoskeleton System for Passive Gait Rehabilitation, IETE Journal of Research, DOI: [10.1080/03772063.2020.1838346](https://doi.org/10.1080/03772063.2020.1838346)

To link to this article: <https://doi.org/10.1080/03772063.2020.1838346>



Published online: 05 Nov 2020.



Submit your article to this journal [↗](#)



Article views: 72




View related articles [↗](#)



View Crossmark data [↗](#)

# Towards Neuro-Fuzzy Compensated PID Control of Lower Extremity Exoskeleton System for Passive Gait Rehabilitation

Jyotindra Narayan  and Santosha Kumar Dwivedy

Mechanical Engineering Department, Indian Institute of Technology Guwahati, Guwahati, Assam 781039, India

## ABSTRACT

The objective of this work is to design a neuro-fuzzy compensated PID control for passive gait rehabilitation using a lower extremity exoskeleton system. A prototype of 6-DOFs exoskeleton device is developed to assist the children of age 8–10 years old. A dummy having a well-matched body attributes to a healthy child (10 years) is utilized in this work to carry out the experimental runs. Kinect-LabVIEW setup is employed to compute the desired joint angles in the sagittal plane for a healthy gait trajectory. The Euler–Lagrange method is utilized to formulate the dynamic analysis of the exoskeleton system. As the performance of existing control strategies for gait rehabilitation devices is still debatable; therefore, a robust neuro-fuzzy compensated PID control strategy is designed in this work. The asymptotic stability of the proposed control scheme is proved mathematically by Lyapunov theorem. Thereafter, the proposed control strategy is implemented on the exoskeleton-dummy setup in real-time and compared with the classical PID control strategy. From experimental runs, the root mean square error (RMSE) for proposed control scheme is found to be less by 40% nearly while tracking the desired gait trajectory. The robustness of the proposed controller is also validated by varying lower limb masses of dummy and by providing an external disturbance. It is observed that proposed controller is more robust to deal with the input disturbance as compared to parametric uncertainty. Finally, the low values of settling time in both the directions ensures the fast convergence of proposed controller.

## KEYWORDS

Euler-Lagrange; External disturbance; Gait rehabilitation; Lower extremity exoskeleton system; Neuro-fuzzy compensated PID; Parametric uncertainty

## 1. INTRODUCTION

Among the elderly people, stroke is considered as a prevalent disease where the functionality of the body parts gets effected. This is due to the seizure of blood flow that carries oxygen and nutrients to the brain [1]. In many cases, stroke leads to impairment of motor nerves and becomes a primary source of mobility loss. As per the reports of the World Health Organization (WHO) [2], the second leading source of death is recorded as stroke with over 5 million cases during 2000–2016 and the third principal basis of disability worldwide [3]. According to a study on the “Global burden of stroke and risk factors in 188 countries, during 1990–2013” [4,5], the environmental factors like air pollution were found to be one of the important criteria for the stroke burden. Among various forms of stroke disabilities, the lower limb disability affects most of the daily living activities (ADLs) due to the loss of healthy gait characteristics. Therefore, to enhance the motor abilities of the lower extremity and recover the healthy gait for the stroke affected population, several rehabilitation measures are being adopted

by physiotherapists [6,7]. Although therapists can perform therapeutic measures based on their knowledge and experiences, more accurate training performances can be achieved by using lower limb robotic-exoskeleton devices with fewer labour efforts.

From the last one and a half decades, various robotic aided lower extremity exoskeleton devices (LEEDs) have been developed to achieve active and passive therapeutic measures [8–10]. Conventionally, LEEDs are classified into three categories based on the application: assistive [10–12], rehabilitation [13–16], and strength augmentation devices [17]. Mohan *et al.* [10] introduced a passive exoskeleton ANKUR-LL II with a RRR configuration, which is augmented to a vertical manipulator having a parallel arrangement of 2PRP-2PPR. This lower extremity exoskeleton system is specifically designed to assist the patients in the sagittal plane. Cestari *et al.* [11] presented an assessment of the compliant actuation system in ATLAS exoskeleton to assist the children during flexion/extension of hip and knee joints. The ankle's

dorsiflexion/plantarflexion movement is delivered via an attached link between the shank and thigh. For the preliminary investigation, a dummy having inertial and mass properties of 10 years human child was utilized to test the exoskeleton system. In another study on assistive exoskeleton devices with active hip, knee and ankle joints, Biomimetic compliant lower extremity exoskeleton robot (BioComEx) has been proposed where a variable stiffness actuator drives the ankle joint, and series elastic actuators (SEAs) drive the knee joint as well as hip joint [12]. Active Leg Exoskeleton (ALEX) [13], as a rehabilitation device, is developed with linear actuators affixed with hip and knee joints. The desired force fields on the moving leg are applied using a force-field controller. For safety purposes, ALEX was tested with a dummy leg having geometrical and inertial parameters similar to the human leg. For rehabilitation purposes, LOKOMAT [14] was introduced with the subject cooperative strategy to avoid repetitive work by the physiotherapists for a long time. Lower Limb Powered Exoskeleton (LOPES) [15], as a treadmill-mounted robotic exoskeleton, has been developed with the active hip joint for the rehabilitation of lower extremity. Long *et al.* [16] proposed a lower extremity exoskeleton device where the knee joint is actuated active-wise, and other ones are actuated using elastic elements. In another work on strength augmentation, Human Power Augmentation Lower Exoskeleton (HUALEX) device [17] is designed with ten DOFs (revolute joint type) where two active joints are actuated with an arrangement of a double-link pendulum. A two-linkage revolute mechanism is employed to keep the arrangement parallel to the human thigh and shank.

The performance of the robot-assisted training for the repetitive tasks is measured at the expense of the control architecture. Control techniques are utilized to mimic the job of manual therapists in a promising manner and achieve the best clinical treatment for the subject during gait rehabilitation. Vasanthkumar *et al.* [18] presented a robust proportional–integral–derivative (PID) control with a disturbance observer scheme for a 1P-2PRP lower extremity rehabilitation manipulator. Hussain *et al.* [19] proposed a sliding mode control based scheme to guide the lower extremity of the subjects on predefined trajectories using a 6-DOFs orthosis device. The controller was found to be effective with three different subjects as a form of structured uncertainties; however, the adaptive feature to assess disability level was not explored. The joint compliance was also controlled for the hip and knee joints in the sagittal plane. In another work on hybrid control, Majeed *et al.* [20] utilized the particle swarm optimized force control scheme to address the disturbance of conventional PD control. The optimal values of

inertial matrix were solved by particle swarm optimization (PSO) method. However, the problem of parametric uncertainty was not discussed extensively. Dao and Yamamoto [21] explained a feedforward-feedback control strategy for pneumatically actuated muscles affixed with a lower extremity rehabilitation device. In a recent work on speed control during gait trajectory tracking [22], a fuzzy-PID control strategy is introduced where fuzzy rules are used to inquire about the PID gain parameters. In another recent work on gait rehabilitation of children, a reference trajectory based Jacobian transpose control approach is proposed by Narayan *et al.* [23]. However, Jacobian transpose control is inefficient to deal with parametric uncertainties and disturbances. ALEX [13,24] has utilized the force-field controller along with a gravity feed-forward scheme to achieve the “assist-as-needed” facility for a dummy leg and the human lower extremity, consecutively. Although many control strategies have been developed for lower extremity exoskeleton devices, there are very few control strategies available to address the parametric uncertainties and unstructured disturbances during the therapeutic training. The change in model parameters (system mass and length) and/or incoming of the disturbances (friction and uneven terrain) during dynamic interaction leads to a significant increase in steady-state error while tracking the gait trajectory. To minimize the steady-state error, large integral gain is required, which eventually degrades the system’s transient response. Therefore, to establish an excellent trade-off between steady-state error and transient response, a novel trajectory tracking control is proposed in this work by incorporating a neuro-fuzzy compensator along with a classical PID controller. To the authors’ best knowledge, this control strategy is not yet explored for passive gait rehabilitation by lower extremity exoskeleton robot.

This paper aims to design a neuro-fuzzy compensated PID control strategy for passive gait rehabilitation of children using a lower extremity exoskeleton robotic device. To address the objective, an experimental setup of 6-DOFs lower extremity exoskeleton is considered with a dummy having geometrical, mass, and inertial properties equivalent to 10 years healthy human child. The desired joint angles and associated gait trajectory for the right lower extremity of 10 years old child in the sagittal plane are exploited as controlled parameters. The dynamic analysis for the right extremity of the exoskeleton system is presented using the Lagrangian method. The neuro-fuzzy compensated PID control scheme is designed and deployed into the experimental setup of the exoskeleton device. Thereafter, to validate the robustness of the neuro-fuzzy compensated PID control, two cases

are considered. In the first one, parametric uncertainty is incorporated by increasing 30% of lower extremity masses of child dummy and in the second case, external disturbance is provided by inducing friction torque model into the dynamics of the system. At last, a comparative analysis between the tracking results of PID control and neuro-fuzzy compensated PID control is carried out using statistical tools.

The organization of the paper is as follows. In Section 2, a description of LEES design, desired trajectory, and real-time control architecture is presented. In Section 3, a dynamic analysis of the LEES, along with the dummy, is performed. In Section 4, the working principle of a conventional PID controller for LEES's experimental setup is described. In Section 5, the design of the neuro-fuzzy compensator, details of the training dataset and stability, is extensively presented. Thereafter, the results of the proposed control strategy for passive gait rehabilitation using LEES are discussed in Section 6. At last, in Section 7, the conclusions for the current work are presented.

## 2. SYSTEM DESCRIPTION

### 2.1 . Design Specification of LEES

The design considerations of a lower extremity exoskeleton system always demand for strength, stability, and safety aspects for the subject. To ensure the strength with minimal system weight and cost, lightweight aluminium materials are used to develop the exoskeleton system. The system's structural stability is maintained by allowing hip, knee, and ankle joint movements in the sagittal plane only. Although increasing degrees of freedom (DOFs), more than one for each lower limb joint provides more flexibility to the subject; however, it could be the reason for involuntary movements and impart discomfort to the subject. Moreover, the safety and postural balance of the subject is also guaranteed by developing a stand-support module on the wheels. Invoking above mentioned design aspects in the SolidWorks interface, a 6-DOFs lower extremity exoskeleton is designed, as shown in Figure 1. Thereafter, a proof-of-concept derived prototype is developed in the Mechatronics and Robotics Laboratory of the institute, as shown in Figure 2.

Each leg of the exoskeleton is made up of three links: thigh link, calf link, and foot link affixed with each other using three revolute joints. Every joint (hip, knee, and ankle), having one degree of freedom and allowing movement in the sagittal plane, constitute 3-DOFs linkage mechanism in one leg. Hip and knee joint favours

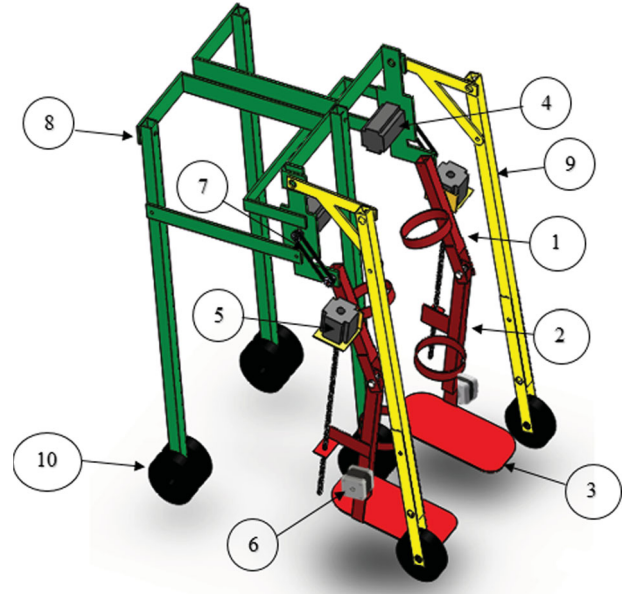


**Figure 1:** CAD model of LEES (Labels: 1. Thigh link, 2. Knee link, 3. Foot link, 4. Hybrid stepper motor, 5. Lead screw actuator, 6. Stepper motor, 7. Timing belt 8. Stand structure, 9. Front support and 10. Stand wheels)



**Figure 2:** Experimental prototype of LEES with child dummy



**Table 1: Range of motion (ROM) for lower limb exoskeleton system and child dummy**

Lower Limb Exoskeleton System			Child dummy		
Joint	Hip (f/e)	Knee (f/e)	Ankle (d/p)	Hip (f/e)	Knee (f/e)
ROM	30/−20	70/−10	5/−15	27/−13	62/−5
					Ankle (d/p)
					2/−8

flexion/extension (f/e) movements, while ankle joint performs dorsiflexion/plantarflexion (d/p) movements throughout a gait cycle. A pair of heavy-duty stepper motors is used to drive the hip joints of both legs via timing belt-pulley arrangements with a transmission ratio of 1. This arrangement is made to avoid shaft bending of the hip joints due to the gradual load of actuators. For the actuation of knee joints, pair of leadscrew type stepper motors are used by affixing them onto the thigh and calf links. A relation between the translational length of the leadscrew and knee joint angle is established using the cosine formula. Ankle joints are actuated using a pair of light-duty stepper motors having less rated output. The DC stepper motor-based actuation drives are selected over hydraulic and pneumatic actuation drives to reduce the installation complexity and ease the exoskeleton system's portability.

The proposed LEES is designed and developed for healthy children having body parameters as age: 8–10 years, weight: 25–35 kg and height: 110–120 cm where being healthy refers to no impairment in the motor functionality. Accounting for the user's physiological safety, the maximum allowable range of motion (ROM) for hip, knee, and ankle joints of the LEES are selected as per studies [25,26], as shown in Table 1. The joints' ROM acts as trajectory constraints and setup the movement limitations for the user. An emergency stop/shut-down button is installed in both software and hardware interfaces to avoid any involuntary ROM or out of the specified maximum ROM while applying the control strategy. As shown in Figure 2, a child dummy with 26 kg weight and 112 cm height is utilized to validate the system's effectiveness and safety measures. A detailed weight, length, and centre of mass (COM) specifications for lower extremity exoskeleton system and the dummy is shown in Table 2. The lower extremities of the dummy are affixed to the leg links of exoskeleton robot using Tynor splints/white tapes. As the dummy cannot apply resistive forces to the exoskeleton system, gait rehabilitation measures are considered passive.

## 2.2 Computation of Desired Trajectory

The passive gait rehabilitation of a human child requires the desired trajectory to be followed and controlled by

**Table 2: Specifications of lower limb exoskeleton system and child dummy**

Lower Limb Exoskeleton System			
Part	Weight (Kg)	Length (m)	COM (m)
Thigh link	4.75	0.30	0.12
Calf link	1.60	0.28	0.11
Foot link	0.85	0.15	0.07

Child Dummy			
Part	Weight (Kg)	Length (m)	COM (m)
Thigh	3.50	0.28	0.14
Calf	2.25	0.25	0.12
Foot	0.65	0.12	0.06

the exoskeleton system. Wireless experimental setup of Microsoft Kinect [27] and NI-Labview [28] was installed to compute the biomechanical joint angles of right and left lower limb in the sagittal plane. With necessary permission, a healthy human child having age 10 years old, 30 kg weight, and 112 cm height was asked to follow an inclined path in front of Kinect camera for at least one gait cycle. The Kinect system was placed at an altitude of 0.8 m from the ground level. The horizontal and vertical distance between the device centre and the child starting point was 0.7 and 2.2 m, respectively. Kinesthesia toolkit [29] within NI-LabVIEW provides instant accessibility of information regarding Kinect camera and skeletal tracking. After accessing skeletal data, lower extremity joint angles were computed using Euclidean distances between joint triples and cosine formula. A detailed procedure to evaluate hip, knee, and ankle joint angles in the sagittal plane using MS-Kinect based NI-LabVIEW setup is presented by Narayan *et al.* [30]. After evaluating joint angles of the right lower limb, the associated gait trajectories were assessed using the LEES kinematics. A complete process flowchart to achieve the desired trajectory of the lower extremity is shown in Figure 3.

## 2.3 Real-Time Control Architecture

In real-time, the control architecture is designed with hardware components like DC motors, motor drivers, voltage source, data boards, feedback sensors, and a host computer to follow the desired gait trajectory. The proposed control strategy is setup into MATLAB/Simulink (2019b, Mathworks) with Arduino Hardware Support Package installed on the host computer. Prior to gait training therapy, the desired trajectory and participating joints should be selected in the software-hardware interaction interface by the administrator. Motor drivers control DC motors by providing precisely regulated voltage received from the voltage source. The control strategy output is first sent to Arduino data boards in the

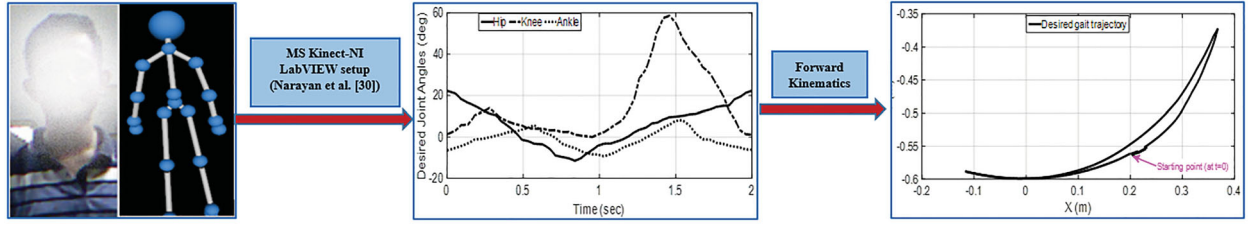


Figure 3: Computation of desired lower limb joint angles and desired gait trajectory

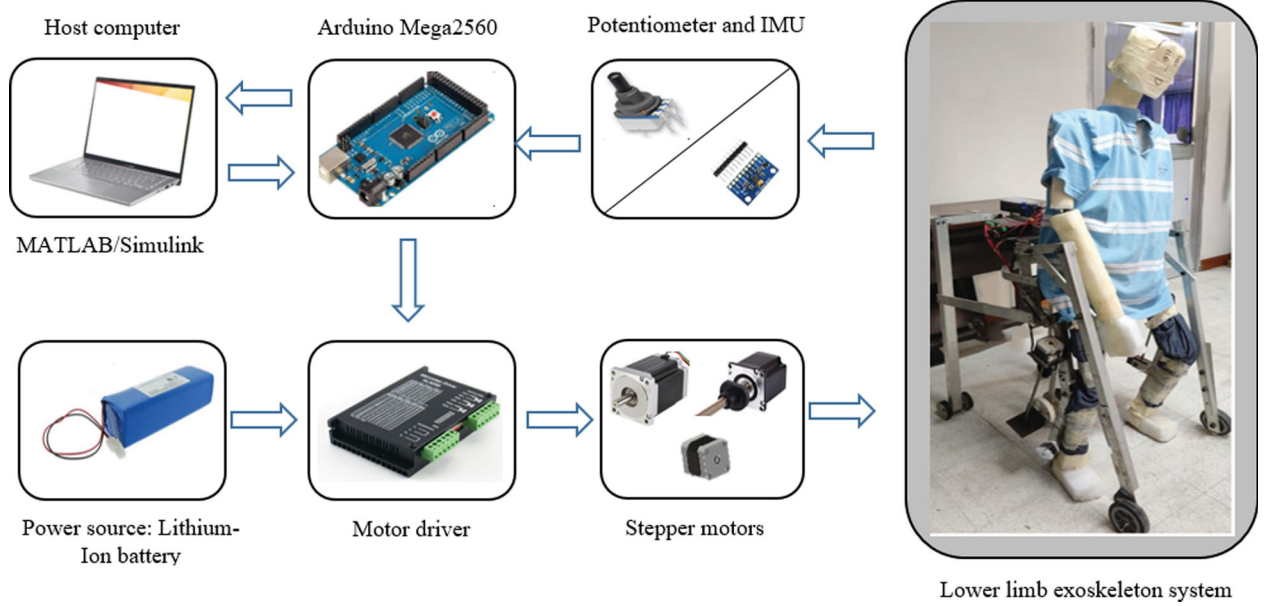


Figure 4: Real time control architecture for the experimental setup

form of pulse width modulations (PWMs) and thereafter inputted to the motor drivers for the voltage regulation of DC motors. The joint angles are measured using potentiometers at the hip and ankle joint shaft and inertial motion unit sensors at the calf link. Thereafter, these angles are sent back to the control strategy as closed-loop feedback via data boards. The communication between the host computer and Arduino data board is established via a USB cable. The block diagram of the hardware components, forming the real-time control architecture with the experimental setup, is presented in Figure 4.

### 3. DYNAMIC MODELLING OF THE LOWER EXTREMITY EXOSKELETON SYSTEM

The dynamic model presents a mathematical relation between employed joint torques and generated joint angular acceleration of LEES. The mathematical description is exploited to realize the dynamics of experimental setup while applying a control strategy. To formulate the system dynamics of any kind, several methods are

available in the literature *viz.* Newton-Euler formulation, Kane method, Lagrangian approach, and Hamilton theory. However, among these methods, the Lagrangian approach and Newton-Euler formulation are extensively used to design a control system [31]. Lagrange method analyses the system energy while Newton-Euler concentrates on the system force to model the dynamics. In this work, the Lagrange method [32] is used to model the dynamics of the lower extremity exoskeleton system in the sagittal plane. A simplified 3-DOFs mechanism with three planar linkages can be considered for one leg, as shown in Figure 5. The Lagrangian function  $L$  and the generalized Lagrange formulation to evaluate joint torques are described as:

$$\tau = \frac{d}{dt} \left( \frac{\partial L}{\partial \dot{\theta}_i} \right) - \frac{\partial L}{\partial \theta_i} \quad (1)$$

$$L = K - P \quad (2)$$

where  $\theta_i$  ( $i = 1, 2, 3$ ) denotes the generalized coordinates for the system,  $\tau$  symbolizes the joint torque vector,  $K$  is the total kinetic energy of the system, and  $P$  is the potential energy of the system.

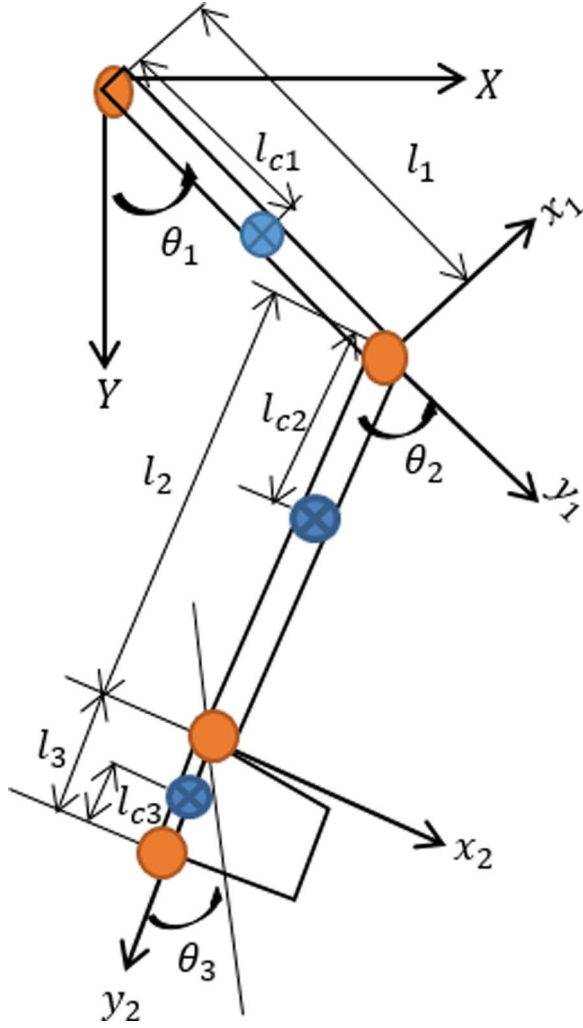


**Figure 5:** A 3-DOFs lower limb mechanism

The kinetic energy of the  $i$ -link is calculated as,

$$K = \sum_{i=0}^3 \left( \frac{1}{2} m_i \dot{\mathbf{s}}_i^T \dot{\mathbf{s}}_i + \frac{1}{2} \dot{\theta}_i^T \mathbf{I}_i \dot{\theta}_i \right) \quad (3)$$

where  $m_i$  denotes the mass of the  $i$ -link,  $\dot{\mathbf{s}}_i$  represents the translational speed of the centre of mass of the  $i$ -link,  $\mathbf{I}_i$  is the inertia matrix of the  $i$ -link, and  $\dot{\theta}_i$  signifies the angular speed of the  $i$ -link.

The potential energy of the  $i$ -link is calculated as,

$$P = \sum_{i=0}^3 (m_i g h_{ci}) \quad (4)$$

where  $m_i$  is the mass for the  $i$ -link,  $g$  is the acceleration due to gravity, and  $h_{ci}$  is the distance from the starting point (origin) to the centre of the  $i$ -link parallel to the gravity vector.

Substituting Equation (3) and Equation (4) into Equation (2) and thereafter solving Equation (1), the matrix presentation for a single leg dynamics of LEES can be formulated as:

$$\boldsymbol{\tau} = \mathbf{M}(\boldsymbol{\theta})\ddot{\boldsymbol{\theta}} + \mathbf{C}(\boldsymbol{\theta}, \dot{\boldsymbol{\theta}})\dot{\boldsymbol{\theta}} + \mathbf{G}(\boldsymbol{\theta}) \quad (5)$$

where  $\mathbf{M}(\boldsymbol{\theta}) = \begin{bmatrix} M_{11} & M_{12} & M_{13} \\ M_{21} & M_{22} & M_{23} \\ M_{31} & M_{32} & M_{33} \end{bmatrix}$ ,  $\mathbf{C}(\boldsymbol{\theta}, \dot{\boldsymbol{\theta}}) = \begin{bmatrix} C_{11} & C_{12} & C_{13} \\ C_{21} & C_{22} & C_{23} \\ C_{31} & C_{32} & C_{33} \end{bmatrix}$  and  $\mathbf{G}(\boldsymbol{\theta}) = \begin{bmatrix} G_1 \\ G_2 \\ G_3 \end{bmatrix}$ .

In the Equation (5),  $\boldsymbol{\tau}$  denotes the vector of the actuator torques,  $\mathbf{M}(\boldsymbol{\theta})$  represents the  $3 \times 3$  total inertia matrix,  $\mathbf{C}(\boldsymbol{\theta}, \dot{\boldsymbol{\theta}})$  denotes the effect of Coriolis and centrifugal forces in  $3 \times 3$  matrix,  $\mathbf{G}(\boldsymbol{\theta})$  refers the gravitational effect in  $3 \times 1$  matrix, and  $\boldsymbol{\theta}$  indicates the joint angles in vector form,  $\dot{\boldsymbol{\theta}}$  denotes the joint angular velocity in vector form,  $\ddot{\boldsymbol{\theta}}$  symbolizes the joint angular acceleration in vector form.

#### 4. CONVENTIONAL PID CONTROLLER

A classical PID control strategy is briefly explained based on three well-known attributes: the first one where stable response action is monitored by the proportional control with converging steady-state error, the second one where the steady-state error is kept minimum using the integral control, and the third one where the settling time is improved using the derivative control after estimation of the errors' in future [31]. The PID controller is conventionally opted due to the simplicity in application and the sustainable performance in different processes. The parallel structure of PID is utilized in a continuous-time domain and has the following mathematical form:

$$U(t)_{PID} = K_p e_\theta(t) + K_i \int e_\theta dt + K_d \frac{de_\theta}{dt} \quad (6)$$

$$e_\theta(t) = \theta_d(t) - \theta_a(t) \quad (7)$$

where  $U_{PID}$  denotes controller output,  $e_\theta$  signifies angular error due to the difference between the desired and actual joint position,  $\theta_d$  is the desired joint position,  $\theta_a$  is the actual joint position, and  $K_p, K_i, K_d$  denotes the proportional, integral and derivative controller gains, respectively.

As shown in Figure 6, PID control is employed to minimize the Cartesian error at the tip of the exoskeleton foot while tracking a healthy gait trajectory during passive rehabilitation. The first step is to calculate the difference between the desired and the actual joint angle

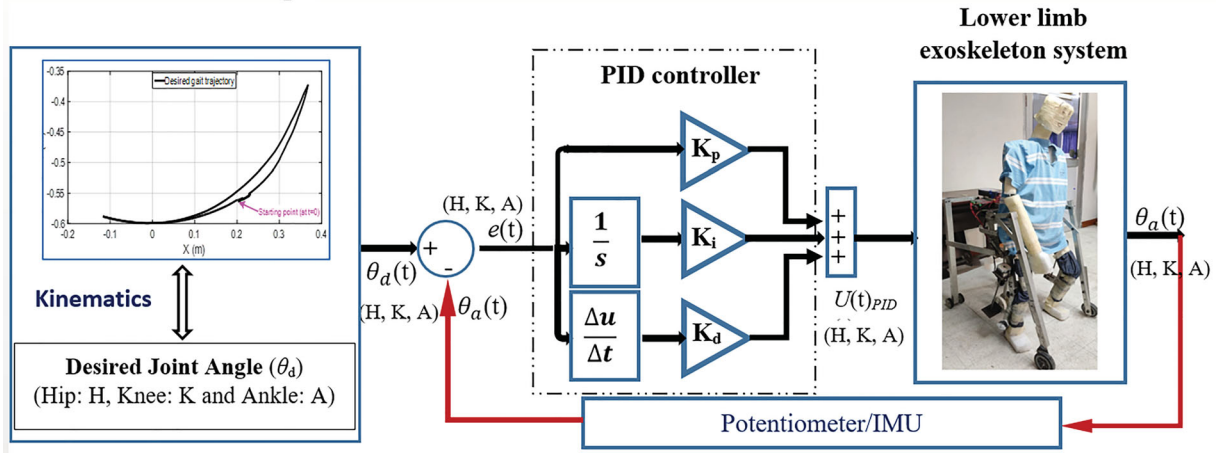


Figure 6: Conventional PID control strategy for LLES

values and defined as the error signal. Thereafter, this signal is provided to the PID controller with tuned proportional ( $K_p$ ), integral ( $K_i$ ), and derivative ( $K_d$ ) gains. Several numerical experiments are performed with different combinations of proportional, integral, and derivative gains for proposed control law. The controller output, applied at the actuator, is further inputted to the LEES dynamics and provides the angular acceleration. A linear relationship is assumed between two forms of controller output, which means voltage in experimental setup and torque in dynamic formulations is considered equivalent. Thereafter, angular acceleration is integrated two times to achieve the actual joint rotation angle. The complete procedure is repeated over and over again until the error touches to a minimum value. However, when the unknown dynamic uncertainties are big, integral gain ( $K_i$ ) needs to be magnified to ensure asymptotic stability. With large values of integral gain ( $K_i$ ), the system may realize high overshoot and bad stability. Therefore, to maintain an effective balance between minimal overshoot and maximum stability, an adaptive neuro-fuzzy inference system (ANFIS) based model-free compensator is proposed in the next section along with the PID controller.

## 5. NEURO-FUZZY COMPENSATED PID CONTROLLER

In this section, a hybrid intelligent based position controller, as a combination of neuro-fuzzy compensator and proportional–integral–derivative (PID) controller, is proposed to control the lower extremity exoskeleton robot. To ensure improved control performance, many neural and neural-fuzzy based adaptive control strategies have been exploited to control robotic systems [33,34] and improve smart home appliances [35]. However,

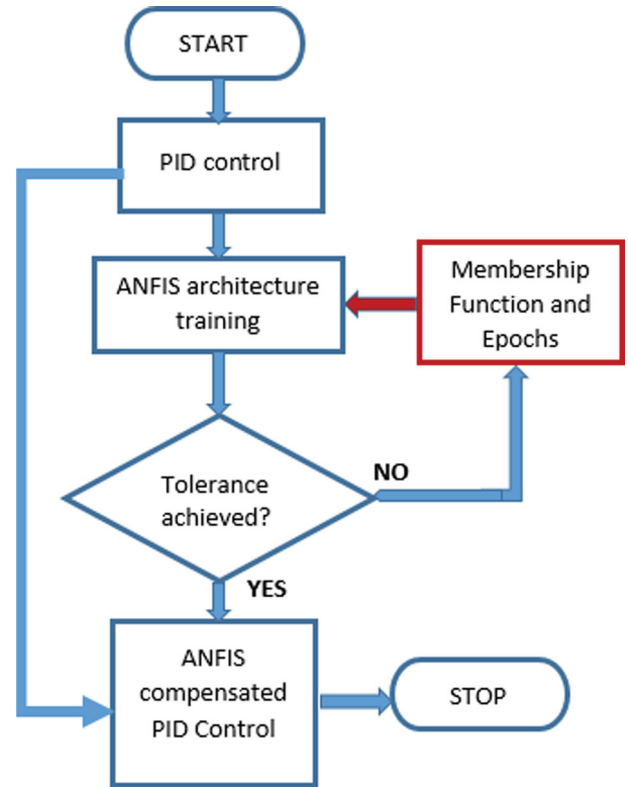


Figure 7: Process flowchart of neuro-fuzzy compensated PID controller

model free intelligent schemes are yet to be significantly explored to control the lower extremity exoskeleton system. The learning characteristic of the ANFIS based compensator is devoted to overcome the parametric uncertainty and unstructured disturbances. On the other hand, the PID controller is utilized to reduce the positional tracking error during passive gait rehabilitation. A process flowchart for the proposed neuro-fuzzy compensated PID controller is shown in Figure 7.



## 5.1 Adaptive Neuro-Fuzzy Inference System (ANFIS)

Established by Jang [36], the adaptive neuro-fuzzy inference system (ANFIS), simply known as the neuro-fuzzy approach, primarily utilizes the key features of neural network and fuzzy logic. The neural network offers the approximation of nonlinear function while regulating the premise and subsequent bounds. Additionally, fuzzy logic is exploited to build IF-THEN rules using input-output datasets. The design architecture of the ANFIS approach comprises of five layers: node layer, membership layer, rule layer, defuzzification layer, and output layer. There are nodes and directional links associated with each layer. The circular nodes are considered as fixed, and the square nodes are considered as adaptive, as illustrated in Figure 8.

### 5.1.1 First Layer: Node Layer

In this layer, nodes of an adaptive kind are used with output functions. The degree of inputs' membership is decided by employing premise bounds to the provided quantifier. The output of adaptive nodes in this layer can be summarised as:

$$O_j^1 = v_{P_j}(I_1), O_j^1 = v_{Q_j}(I_2) \quad (8)$$

where  $O_j^i$  denotes the node output at  $j$ -th position corresponding to  $i$ -th layer,  $v_{P_j}, v_{Q_j}$  indicates the membership function for the respective input, and  $\{I_1, I_2\}$  represents the input vectors.

### 5.1.2 Second Layer: Membership Layer

This layer comprises of fixed nodes with output functions. The firing strength of rule is established by having a multiplication of distinct inward membership functions from the preceding layer. The layer output associates the input of the consequent layer and provided as:

$$O_j^2 = \varphi_j = v_{P_j}(I_1) \times v_{Q_j}(I_2), j = 1, 2, 3. \quad (9)$$

### 5.1.3 Third Layer: Rule Layer

In this layer, the firing strength is normalized using the output function of every fixed node. The normalization process is carried out by evaluating every activation level's dividend with respect to the sum of all activation levels. The output of the rule layer associates the membership layer in the form of activation levels and can be depicted as:

$$O_j^3 = \bar{\varphi}_j = \frac{\varphi_j}{\varphi_1 + \varphi_2 + \varphi_3} \quad (10)$$

### 5.1.4 Fourth Layer: Defuzzification Layer

Adaptive nodes are utilized in this layer to evaluate the contribution of rules by defuzzification of input vectors

as follows:

$$O_j^4 = \bar{\varphi}_j f_j = \bar{\varphi}_j(u_j I_1 + v_j I_2 + r_j) \quad (11)$$

where  $\bar{\varphi}_j$  signifies the output of rule layer and  $\{u_j, v_j, r_j\}$  represents the subsequent bounds. The input elements  $I_1, I_2$  are instituted by IF-THEN rules, following the fuzzy system of Takagi and Sugeno's type, as follows:

If  $I_1$  is  $M$  and  $I_2$  is  $N$ , then  $f = (pM + qN + r)$ .

where  $M$  and  $N$  denote fuzzy sets and  $u, v, r$  symbolizes the design parameters retrieved from the training procedure.

### 5.1.5 Fifth Layer: Output Layer

Exploiting this layer, overall output is provided by having a summation of all input signals and expressed as follows:

$$O_j^5 = \sum_j \bar{\varphi}_j f_j = \frac{\sum_j \varphi_j f_j}{\sum_j \varphi_j} \quad (12)$$

In literature, several types of membership functions are available to train the neuro-fuzzy network [37]. Being smooth around the corners and having a symmetrical curve around the vertical axis, generalized bell membership functions (MF) are exploited in this work to the design the ANFIS architecture. The bell-shaped MF comprises of an extra parameter to tune the steepness at crossover points as compared to Gaussian MF. The effectiveness of MF is established by changing the number of MF and associated epochs for each input-output training dataset while performing passive gait rehabilitation.

### 5.1.6 Generalized Bell Membership Function

The generalized bell MF follows the mathematical property of a bell-shaped curve with a symmetrical axis, as provided in Equation (13). It consists of three design parameters, i.e. "a", "b", and "c" that indicates the width, shape, and centre of the MF curve. In the expression, "b" is generally positive; however, it could be negative for an inverted bell-shaped curve.

$$bell(I; a_j, b_j, c_j) = v_{P_j}(I_1) = v_{Q_j}(I_2) = \frac{1}{1 + \left(\frac{|I - c_j|}{a_j}\right)^{2b_j}} \quad (13)$$

where  $I: \{I_1, I_2\}$  represents the set of input vectors.

## 5.2 Design of Neuro-Fuzzy Compensated PID Control Strategy

In the design of the proposed controller, the desired gait trajectory and joint angles of the right lower extremity

share a correspondence relation, as shown in Figure 8. A set of potentiometers/IMU sensors are employed to estimate the actual position of joints. Thereafter, two control actions are carried out to generate the control signal (controller output). First, the difference between the desired and actual joint angles, as an error, is fed to the PID controller; and second, the desired joint angles along with the derivatives are provided into already trained ANFIS structure. The former controller action ensures minimal tracking error during gait rehabilitation while the latter one deals with parametric uncertainties and unstructured disturbances by compensating the response of the former one. The combined effect of both control actions is summarized in Equation (14), which collectively drive the exoskeleton device for passive gait trajectory tracking.

$$U(t)_{ACP} = U(t)_{ANFIS} + U(t)_{PID} \quad (14)$$

where  $U(t)_{ACP}$  is the output of the proposed ANFIS compensated PID controller and  $U(t)_{ANFIS}$  is the output of the ANFIS technique.

### 5.2.1 Formation of ANFIS Training Dataset

In the ANFIS training, the input dataset comprises of actual joint angles (hip, knee, and ankle) and the derivative of actual joint angles from the dynamic model. The output dataset consists of a linear distribution of compensating voltages associated with each lower limb joint. The maximum and minimum bound of every linear distribution are defined according to the maximum and minimum output values of the conventional PID controller designed in Section 4. The complete range of three training datasets related to hip, knee, and ankle joints are shown in Table 3. The experimental runs for ANFIS training are performed with a different number of MFs and epochs varying from 1–50 to 1–30. However, it has been noticed that the better results of gait trajectory tracking are found with 15 MFs and 10 epochs for each input, leading to a total of 450 rules

for each training dataset. The two optimization methods are employed in the ANFIS to learn the generated network while training: first, backpropagation and second, hybrid one. The backpropagation method exploits the gradient descent method for error evaluated associated with each node while the hybrid one utilizes the gradient descent along with the least square algorithm to adjust the errors. Therefore, in this work, the latter one is used while training the neuro-fuzzy architecture. The training phase stops as tolerance error approaches to zero.

The block diagram of the proposed neuro-fuzzy compensated PID control strategy for the system dynamics is illustrated in Figure 9. A stepwise design framework for neuro-fuzzy compensated PID control is as follows:

- Step 1: Design of conventional PID controller by tuning of  $K_p, K_i$  and  $K_d$  gains.
- Step 2: Evaluation of PID controller outputs ( $U(t)_{PID}$ ).
- Step 3: Selection of maximum and minimum values of PID controller outputs.
- Step 4: Linear distribution of PID controller outputs.
- Step 5: Formation of ANFIS training dataset
  - Input parameters: actual joint angles ( $\theta$ ) and actual joint angular velocities ( $\dot{\theta}$ ) from dynamic model
  - Output parameters: Linear distribution of PID controller outputs (from step 4)
- Step 6: Training of ANFIS with Gaussian membership function.
- Step 7: ANFIS output ( $U(t)_{ANFIS}$ ) for compensating uncertainties and disturbances.
- Step 8: Combination of ANFIS output from Step 7 and PID output from step 2 to form ANFIS compensated PID as shown in Figure 9 ( $U(t)_{Controller} = U(t)_{ANFIS} + U(t)_{PID}$ ).

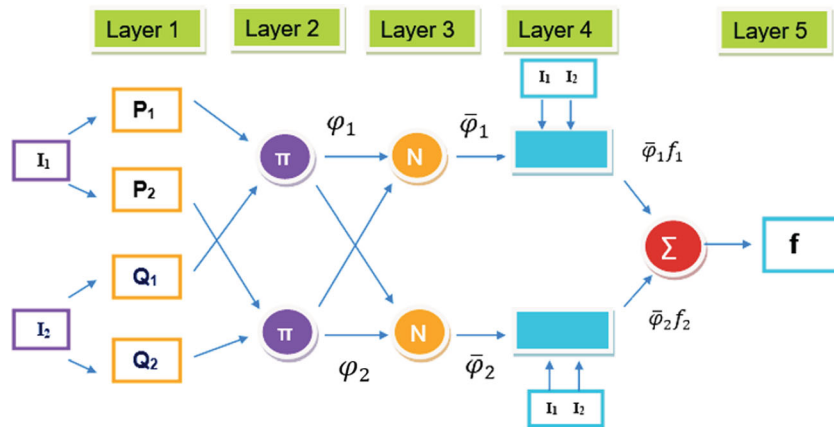
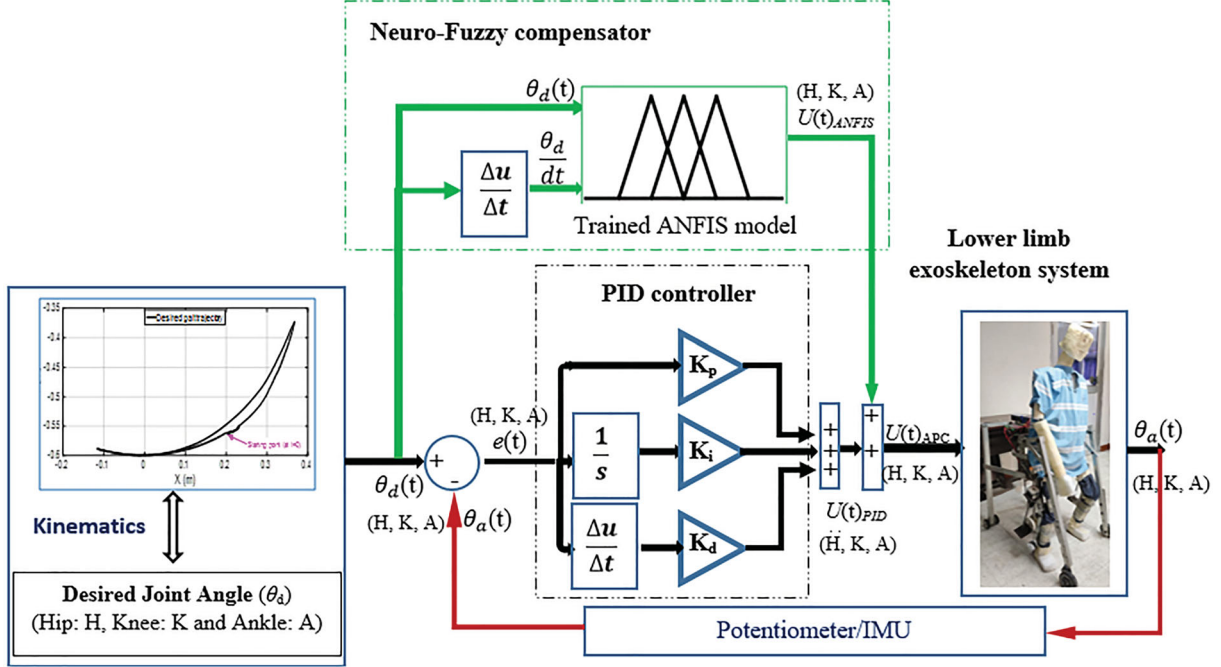


Figure 8: Layers in ANFIS architecture

**Table 3: Input and output training range of ANFIS**

	Actual joint angles (degrees, °)			Derivative of actual joint angles (degrees, °)			Controller output (Voltage, V)		
	Hip	Knee	Ankle	Hip	Knee	Ankle	Hip	Knee	Ankle
	$\theta_H$	$\theta_K$	$\theta_A$	$\dot{\theta}_H$	$\dot{\theta}_K$	$\dot{\theta}_A$	$U_{PIDH}$	$U_{PIDK}$	$U_{PIDA}$
<b>Minimum</b>	-21.52	-10.02	-19.35	-89.21	-177.37	-95.40	-18.16	-7.55	-1.39
<b>Maximum</b>	22.36	78.55	8.15	71.94	247.98	48.23	24.27	11.17	1.21

**Figure 9:** Proposed neuro-fuzzy compensated PID control strategy for LLES

Step 9: Applying the proposed controller output to the exoskeleton dynamics.

### 5.3 Stability of Neuro-Fuzzy Compensated PID Controller

Lyapunov's method of stability is quite popular to confirm the stability of the non-linear dynamic systems [38]. The challenging task associated with non-linear systems is to ensure the closed-form expression for desired trajectories at a given initial state. The two main objectives behind this approach are to achieve a function being minimal at the equilibrium point and to prove the monotonically decreasing nature of the function over a given period of time using system dynamics. The following theorem is proved to guarantee the stability of the proposed ANFIS compensated PID controller.

**Theorem:** Considering the dynamics of lower extremity exoskeleton system (Equation (16)), if the proposed control law (Equation (14)) and adaptive law of weights [39] are employed, the stability of the controller is ensured.

**Proof:** Assume the Lyapunov candidate function based on the tracking error vector ( $\xi$ ) and adjustment for weights ( $\bar{\varphi}$ ),

$$\gamma(t) = \frac{1}{2} \xi^T P \xi + \frac{1}{2} \varsigma^{-1} \text{tr}\{(\bar{\varphi}^* - \bar{\varphi})^T (\bar{\varphi}^* - \bar{\varphi})\} \quad (15)$$

where  $\xi$ :  $[e\dot{e}]$  denotes the tracking error for hip, knee and ankle joint,  $\varsigma$  is a positive constant value,  $\bar{\varphi}^*$  is the optimal set of weights in ANFIS architecture and  $P$  denotes the symmetric positive definite matrix satisfying the relation as

$$PA + A^T P = -Q \quad (16)$$

where,  $A$  is the state matrix having the relation of mass matrix and controller gains and  $Q$  is another symmetric positive definite matrix.

Evaluating the derivative of Lyapunov function  $\gamma(t)$  from Equation (15) as:

$$\dot{\gamma}(t) = \frac{1}{2} \dot{\xi}^T P \xi + \frac{1}{2} \xi^T P \dot{\xi} - \varsigma^{-1} \text{tr}\{(\bar{\varphi}^* - \bar{\varphi})^T \dot{\bar{\varphi}}\} \quad (17)$$

Solving for derivative of tracking error ( $\dot{\xi}$ ) from system dynamics and controller law,

$$\dot{\xi} = A\xi + B\{(\bar{\varphi}^* - \bar{\varphi})^T v\} \quad (18)$$

where  $B$  denotes the inverse of inertia matrix and  $v$  refers to the Gaussian membership function.

Substituting Equations (16) and (18) in Equation (17),

$$\begin{aligned} \dot{\gamma}(t) &= \frac{1}{2}\xi^T(PA + A^TP)\xi + \xi^TPB(\bar{\varphi}^* \\ &\quad - \bar{\varphi})^Tv - \varsigma^{-1}\text{tr}\{(\bar{\varphi}^* - \bar{\varphi})^T\dot{\bar{\varphi}}\} \\ &= -\frac{1}{2}\xi^TQ\xi + \xi^TPB(\bar{\varphi}^* - \bar{\varphi})^Tv \\ &\quad - \varsigma^{-1}\text{tr}\{(\bar{\varphi}^* - \bar{\varphi})^T\dot{\bar{\varphi}}\} \end{aligned} \quad (19)$$

Applying adaptive law of weights from [38], the two sufficient conditions are carried out:

$$\dot{\gamma}(t) = -\frac{1}{2}\xi^TQ\xi \leq 0 \quad (20)$$

and,

$$\dot{\gamma}(t) = -\frac{1}{2}\xi^TQ\xi - \sum_{i=1}^n \left[ \left( 1 - \frac{(\bar{\varphi}_i^*)^T \bar{\varphi}_i}{\bar{\varphi}_i^2} \right) \bar{\varphi}_i^T v \xi^T P B_i \right] \quad (21)$$

where  $n$  is the number of joints of the exoskeleton device,  $\bar{\varphi}_i$  is the initial values of weights and  $\bar{\varphi}_i^*$  is the optimum initial values of weights.

Since  $\left( 1 - \frac{(\bar{\varphi}_i^*)^T \bar{\varphi}_i}{\bar{\varphi}_i^2} \right) \geq 0$ , the Equation (21) can be further modified as

$$\dot{\gamma}(t) \leq -\frac{1}{2}\xi^TQ\xi \leq 0 \quad (22)$$

From Equations (15), (20) and (22), it can be easily observed that  $\dot{\gamma}(t) \geq 0$  and  $\dot{\gamma}(t) \leq 0$ . Moreover, Equation (20) shows that  $\dot{\gamma}(t) = 0$  if and only if  $\xi = 0$  and Equation (21) infers that  $\dot{\gamma}(t) = 0$  if and only if  $\gamma(t) = 0$ . In this manner, the global stability of the ANFIS compensated PID controller is proved. Exploiting Barbalat's lemma [40], it can be also shown that  $\gamma(t) \rightarrow 0$  as  $t \rightarrow \infty$  which ensures the proposed control scheme asymptotically stable.

## 6. RESULTS AND DISCUSSION

In this section, the experiment results and findings of the neuro-fuzzy compensated PID control strategy for

the passive gait rehabilitation using the exoskeleton system. The complete experimental setup is employed in the MATLAB/Simulink environment to validate the effectiveness of the proposed control strategy while comparing with the conventional PID control strategy. To investigate the performance of both the control strategies pertaining to tracking error and required controller output, statistical measures such as the root mean square error (RMSE) and the maximum absolute error (MAXE) are used.

$$RMSE = \sqrt{\frac{1}{N} \sum_{j=1}^N e_j^2} \quad (23)$$

$$MAXE = \max |e_j| \quad (24)$$

where  $e_j$ :  $e_x$  is tracking error in X-direction;  $e_y$  is tracking error in Y-direction;  $e_\theta$  is the joint angular error and  $N$  denotes the number of error data points.

After providing kinematic and dynamic parameters into the applied control schemes, several heuristic based numerical iterations are performed to select the tuned values of  $K_p$ ,  $K_i$ , and  $K_d$ . The value of proportional gain is first altered while keeping the integral and derivative gain constant for converging steady state error. Thereafter, integral gain is increased to remove the residual error and derivative gain is kept constant. Finally, after fixing the proportional and integral gain, the derivative one is tuned to achieve the minimal overshoot in the actual gait trajectory. The respective values are: for hip joint,  $K_p = 300$ ,  $K_i = 10$ ,  $K_d = 50$ ; for knee joint,  $K_p = 300$ ,  $K_i = 10$ ,  $K_d = 40$ ; and for ankle joint,  $K_p = 310$ ,  $K_i = 10$ ,  $K_d = 50$ . Figure 10 presents the comparative analysis of PID and ANFIS compensated PID with respect to the desired gait trajectory over a gait cycle of 2 s. The black line represents the desired trajectory to be followed by the right foot, starting at the left corner with (0.23, -0.56) Cartesian coordinates.

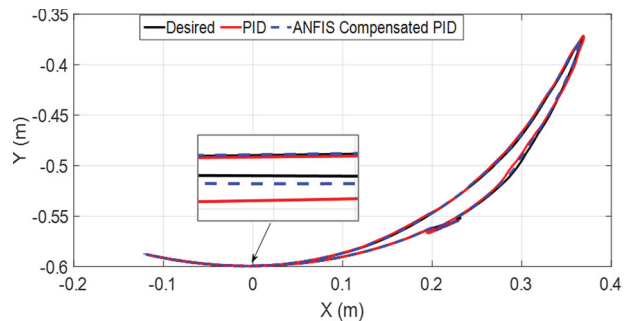


**Figure 10:** Experimental results of trajectory tracking with PID and ANFIS compensated PID control in X-Y plane.



The red line and blue dotted line represents the real-time trajectory covered by the foot after applying the PID and ANFIS compensated PID control strategy trajectory, respectively. To realize the difference between the desired and both the actual trajectories, an enlarged view is illustrated at (0, 0). It can be observed from Figure 11(a) and (b) that the tracking errors in X and Y directions are less for the neuro-fuzzy compensated PID control strategy. On comparing ANFIS compensated PID control strategy with classical PID control strategy, the RMSE value is found to be decreased by 40.42% *i.e.* from 0.94 cm to 0.56 cm in the X-direction and 40.01% *i.e.* from 0.45 cm to 0.27 cm in Y-direction. Moreover, as presented in Table 4, the maximum absolute error (MAXE) in both directions is observed to be less by 57.64% and 59.09% for ANFIS compensated PID control strategy while comparing to simple PID control strategy.

Furthermore, the tracking of the desired hip ( $\theta_H$ ), knee ( $\theta_K$ ), and ankle ( $\theta_A$ ) joint trajectory is illustrated in Figure 12(a), Figure 13(a) and Figure 14(a) after applying PID and ANFIS compensated PID. The real-time joint angles, obtained from the feedback sensors, are devoted to move the LEES along the desired gait trajectory of a human child. Figure 12(b), Figure 13(b), and Figure 14(b) present the angular tracking errors ( $e_{\theta_H}$ ,  $e_{\theta_K}$ ,  $e_{\theta_A}$ ) in the

joint space for the hip, knee, and ankle joint, respectively. As shown in Table 4, the maximum absolute error (MAXE) for hip, knee and ankle joint is reduced by 38.23%, 44.93% and 50.00% with the ANFIS compensated PID control strategy as compared to PID control strategy while tracking the desired joint trajectory.

The required controller outputs ( $U_H$ ,  $U_K$ ,  $U_A$ ), for driving the hip, knee and ankle joints actuators of the lower extremity exoskeleton system, are shown in Figure 15. As shown in Figure 15(a) and (b), the maximum absolute value of the controller output (MAXV) for hip and knee joint is found to be marginally high by 6.36% (25.88 V, 24.27 V) and 14.14% (13.01 V, 11.01 V), respectively with the ANFIS compensated PID control strategy as compared to conventional PID control strategy. However, it can be observed from Figure 15(c), the MAXV for ankle joint is found to be reduced by 13.76% with ANFIS compensated PID control strategy (1.19 V) while compared to conventional PID control strategy (1.38 V).

To validate the robustness of proposed controller with respect to the conventional PID controller, two cases are considered. In first case, as a model parametric uncertainty, a variation in system masses is provided by increasing 30% of thigh, calf and foot masses of child dummy. In second case, an input disturbance in the form

**Table 4: Performance analysis of proposed controller for desired gait trajectory tracking**

Tracking Parameters		Controller Type	Maximum Absolute Error (MAXE) (cm or deg.)	Percentage reduction (%)
Gait Trajectory	X (cm)	Conventional PID	2.86	57.64
		ANFIS compensated PID	1.70	
	Y (cm)	Conventional PID	1.17	59.09
		ANFIS compensated PID	0.72	
Joint Angles	Hip (deg.)	Conventional PID	2.04	38.23
		ANFIS compensated PID	1.26	
	Knee (deg.)	Conventional PID	1.58	44.93
		ANFIS compensated PID	0.87	
	Ankle (deg.)	Conventional PID	0.04	50.00
		ANFIS compensated PID	0.02	

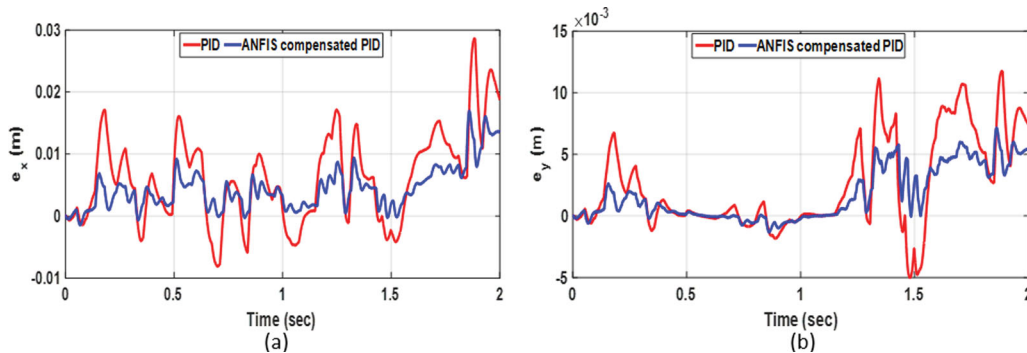


**Figure 11:** Experimental results of tracking error in (a) X-direction. (b) Y-direction

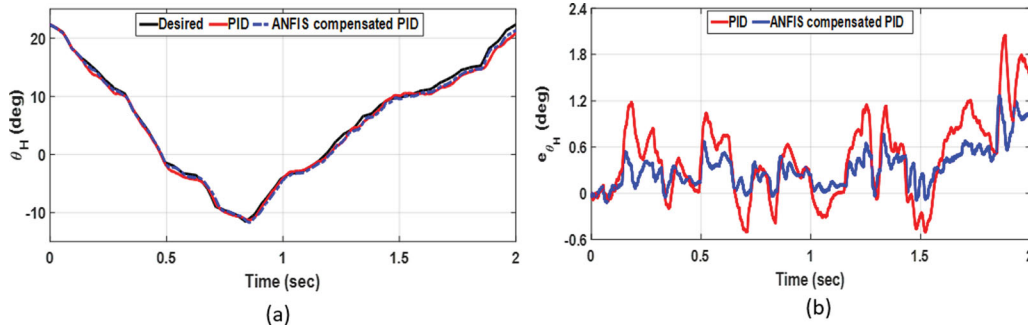


**Figure 12:** Experimental results of (a) hip joint tracking, and (b) hip joint angular error with PID and ANFIS compensated PID control

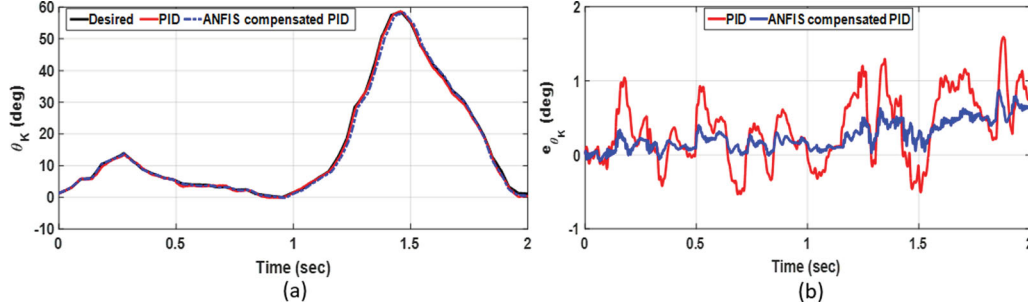


**Figure 13:** Experimental results of (a) knee joint tracking, and (b) knee joint angular error with PID and ANFIS compensated PID control

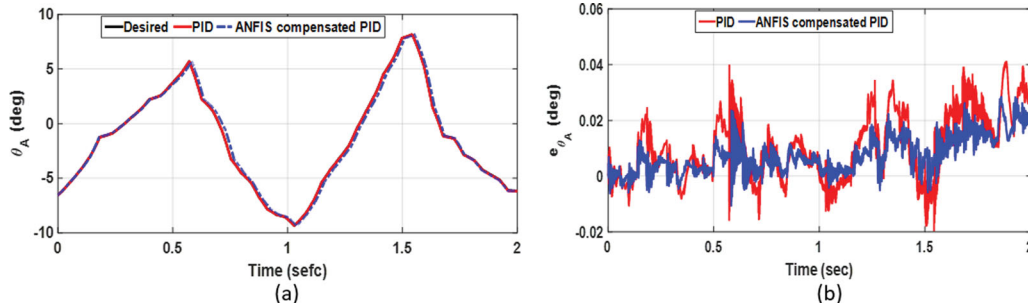


**Figure 14:** Experimental results of (a) ankle joint tracking, and (b) ankle joint angular error with PID and ANFIS compensated PID control

of friction is inputted into the system externally. The friction model encompasses the real-effect of dynamic and steady friction involved in the lower extremity exoskeleton model during gait rehabilitation [32]. The formulation of the input disturbance for each lower limb joint is given in Equation (25) as follows:

$$F_d = F_c \text{sgn}(\dot{\theta}) + \sigma \dot{\theta}, \dot{\theta} \neq 0 \quad (25)$$

where  $F_d$  denotes friction torque model as input disturbance,  $F_c$  is coulomb friction torque,  $\sigma \dot{\theta}$  represents viscous friction torque.

Figure 16 presents the comparative results of PID and ANFIS compensated PID control for increased value of system masses while tracking the desired gait trajectory. It can be shown from Figure 17(a) and (b), the tracking

errors in X and Y directions are still less for neuro-fuzzy compensated control over PID control. Moreover, on comparing the tracking performance of device with original system masses and increased system masses as shown in Table 5, the RMSE value in the X and Y direction for PID control is increased by 58.22% and 56.31%, respectively. On the other hand, for ANFIS compensated PID control, the RMSE value in both the directions is increased by 48.14% and 52.33% which is low as compared to PID control. This ensures the robustness of proposed control against parametric uncertainty.

Moving further, applying the input disturbance from Equation 16 in the system dynamics, a comparative analysis of PID and ANFIS compensated PID control is shown in Figure 18. From Figure 19(a) and (b), very

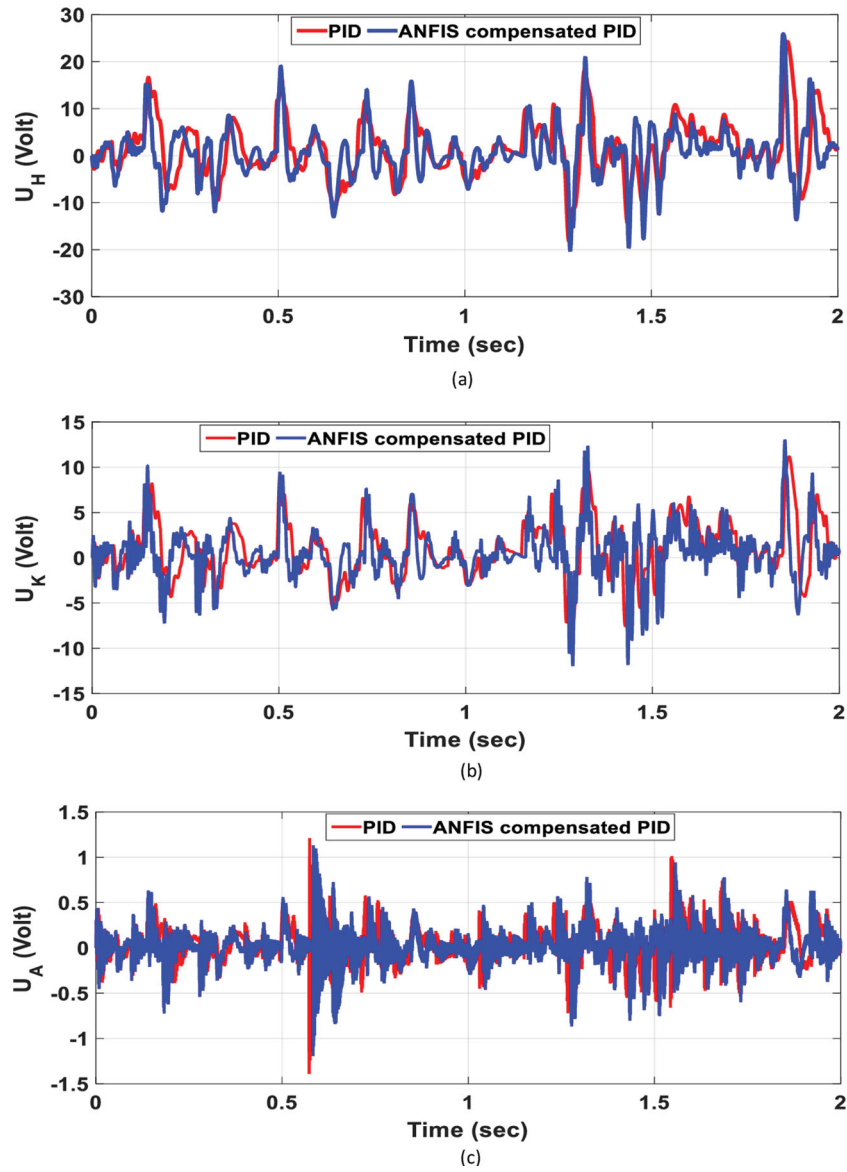


**Figure 15:** Experimental results of controller output at (a) hip joint, (b) knee joint, and (c) ankle joint with PID and ANFIS compensated PID control

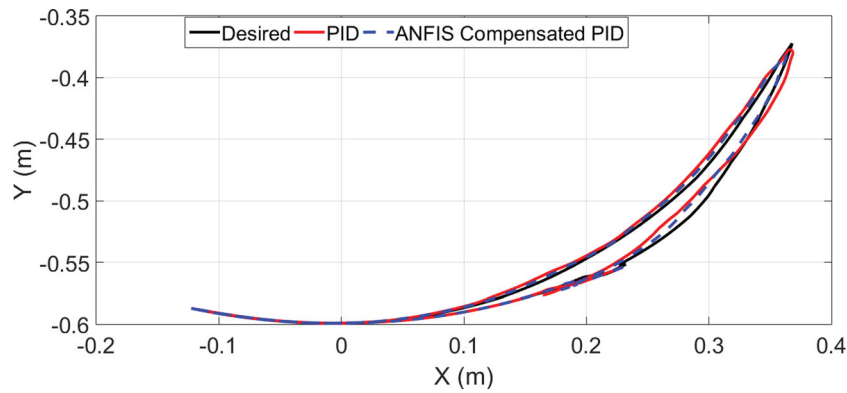


**Figure 16:** Experimental results of trajectory tracking control in X-Y plane for increased system masses.

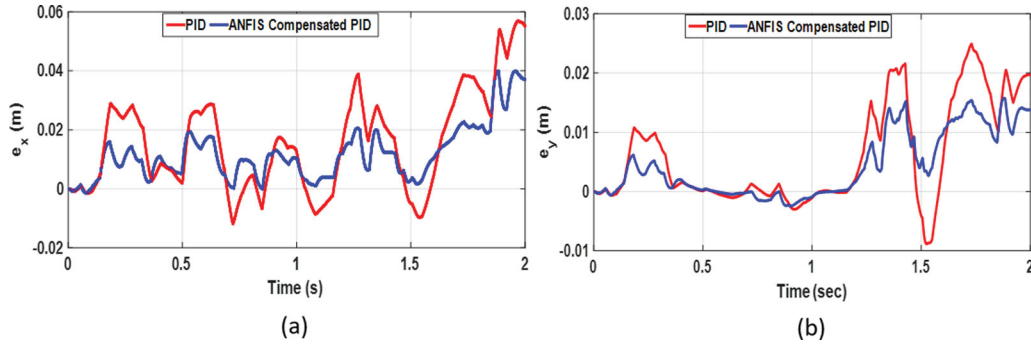


**Figure 17:** Experimental results of tracking error in (a) X-direction (b) Y-direction for increased system masses.

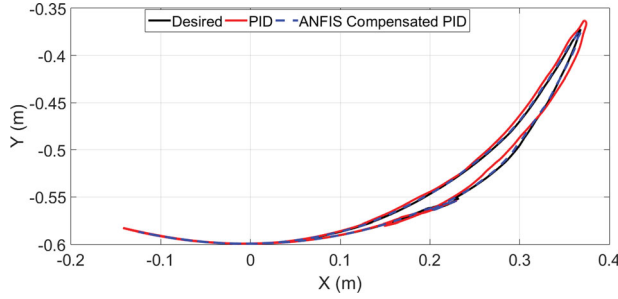


**Figure 18:** Experimental results of trajectory tracking control in X-Y plane with external disturbance.

low tracking errors are found in X and Y directions with neuro-fuzzy compensated control while comparing with PID control. Furthermore, on comparing the tracking performance of the rehabilitation device without any disturbance and with the input disturbance as shown in Table 5, the RMSE value in the X and Y direction for PID

control is drastically increased by 68.35% and 56.73%, respectively. However, for ANFIS compensated PID control, the RMSE value in both the directions is increased by 15.15% and 10.00% which is significantly low as compared to PID control. This guarantees the robustness of proposed control to deal with internal/external disturbances.

Considering mass variation and finding the difference between the percentage rises in RMSE value for both the controllers, the proposed controller is found to be effective by 10.08% and 3.98% in X- and Y-direction as compared to the PID controller. However, with the external disturbance, the same effective difference for proposed controller is found to be 53.2% and 46.73% in X- and Y-directions as compared to the PID controller. Although, from Table 5, it can be easily perceived that ANFIS compensated PID control is more robust than

**Table 5: RMSE values of PID and ANFIS compensated PID for robustness analysis**

Controller Type	Tracking Direction	Robustness validations		
		Original system without external disturbance	Case 1: Increased mass values by 30%	Case 2: External friction disturbance
PID controller	X(cm)	0.94	2.25 (58.22% ↑)	2.97 (68.35% ↑)
	Y(cm)	0.45	1.03 (56.31% ↑)	1.04 (56.73% ↑)
ANFIS compensated PID controller	X(cm)	0.56	1.08 (48.14% ↑)	0.66 (15.15% ↑)
	Y(cm)	0.27	0.57 (52.63% ↑)	0.30 (10.00% ↑)

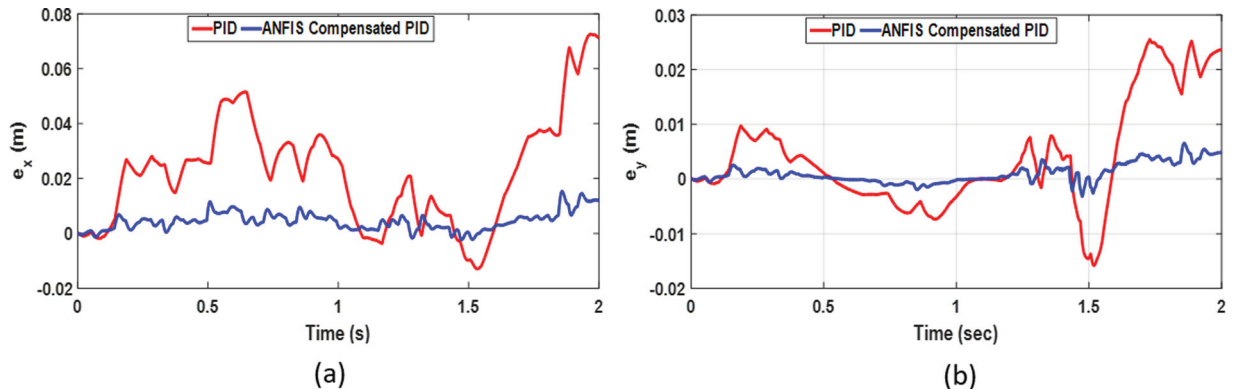


**Figure 19:** Experimental results of tracking error in (a) X-direction (b) Y-direction with external disturbance.



**Table 6: Settling time of PID and ANFIS compensated PID for convergence analysis**

Controller Type	Tracking Direction	Settling time (sec)		
		Original system without external disturbance	Case 1: Increased mass values by 30%	Case 2: External friction disturbance
PID controller	X(cm)	1.941	1.981	1.962
	Y(cm)	1.925	1.965	1.993
ANFIS compensated PID controller	X(cm)	1.903	1.971	1.938
	Y(cm)	1.894	1.957	1.926

conventional PID control with both parametric uncertainty and external input disturbance, however, showing noteworthy robustness towards the latter one. Furthermore, in Table 6, the settling time *i.e.* the time elapsed for the error in X- and Y-direction to fall within 2% of the final value is presented. It is worth noted that the settling time for ANFIS compensated PID control is comparatively less than conventional PID control. This ensures the fast converging behaviour of proposed controller before getting stable.

## 7. CONCLUSIONS

In this work, a neuro-fuzzy compensator aided with a conventional PID controller has been designed and implemented on a lower extremity exoskeleton system for passive gait rehabilitation. An experimental prototype of the lower extremity exoskeleton system has been presented with real-time control architecture. A dummy with geometrical, mass, and inertial attributes similar to a healthy child of age ten years old, has been considered for experiments. A Kinect-Labview setup has been utilized to evaluate the desired joint angles and range of motion for a healthy human child. The Euler-Lagrange method has been employed to describe the dynamic analysis of the lower extremity exoskeleton system. Thereafter, a robust neuro-fuzzy compensated PID control has been designed to deal with parametric uncertainties and external disturbances. The stability of the proposed control has been proved mathematically by Lyapunov theorem. From the experimental runs, it has been observed that the RMSE value in both X- and Y-directions has found to approximately 40% less as compared with conventional PID control. To validate the controller robustness, variation of lower extremity mass by 30% and a friction based external disturbance have been considered. With mass variation, although a rise of 48.14% and 52.33% in RMSE value has been noticed in the respective directions from ANFIS compensated PID control, however still less than the rise of 58.22% and 56.31% from PID control. Similarly, considering the external disturbance, the RMSE value has been increased by 15.15% and 10% in respective directions with ANFIS compensated PID control, however significantly less than the 68.35% and 56.73% with the

PID control. This has ensured more robustness of proposed control with the external disturbance as compared to parametric uncertainty. At last, the rapid convergence of the proposed controller has been guaranteed with the low settling time for all the experimental runs. In future, the work could be extended for robust “assist-as-need” control to address the corrective feedback of the healthy and paraplegic patients.

## ACKNOWLEDGEMENTS

The authors acknowledge the Department of Scientific and Industrial Research, India, for starting the initiative PRISM (Promoting Innovations in Individuals, Start-ups and MSMEs) under which this project is carried out. The authors are also grateful to the amiable support of Mr. Monuranjan Dowarah from Mechatronics and Robotics Laboratory, IIT Guwahati, in performing the research experiments.

## ORCID

Jyotindra Narayan  <http://orcid.org/0000-0002-2499-6039>

## REFERENCES

1. A. G. Rudd, A. Bowen, G. R. Young, and M. A. James, “The latest national clinical guideline for stroke,” *J. Clin. Med.*, Vol. 17, pp. 154, Apr. 2017.
2. World Health Organization, Global Health Estimates 2016. *Deaths by Cause, Age, Sex, by Country and by Region, 2000-2016*. Geneva: WHO, 2018.
3. V. L. Feigin, M. H. Forouzanfar, R. Krishnamurthi, G. A. Mensah, M. Connor, D. A. Bennett, A. E. Moran, R. L. Sacco, L. Anderson, and T. Truelsen, “Global and regional burden of stroke during 1990–2010: findings from the global burden of disease study 2010,” *Lancet*, Vol. 383, pp. 245–55, Jan. 2014.
4. V. L. Feigin, et al., “Global burden of stroke and risk factors in 188 countries, during 1990–2013: a systematic analysis for the global burden of disease study 2013,” *Lancet Neurol.*, Vol. 15, pp. 913–24, Aug. 2016.
5. About Stroke. Available from: <https://www.stroke.org/en/about-stroke>, 2019, [cited: 27 May 2020].
6. P. Langhorne, F. Coupar, and A. Pollock, “Motor recovery after stroke: a systematic review,” *Lancet Neurol.*, Vol. 8, pp. 741–54, Aug. 2009.

7. K. Probosz, R. Wcislo, J. Otfinowski, R. Slota, J. Kitowski, M. Pisula, and A. Sobczyk, "A multimedia holistic rehabilitation method for patients after stroke," *Annu. Rev. CyberTherapy Telemed*, Vol. 7, pp. 261–3, Jun. 2009.
8. K. Lo, M. Stephenson, and C. Lockwood, "Effectiveness of robotic assisted rehabilitation for mobility and functional ability in adult stroke patients: a systematic review protocol," *JBI. Database. System. Rev. Implement. Rep.*, Vol. 15, pp. 3049–91, Dec. 2017.
9. B. Kalita, J. Narayan, and S. K. Dwivedy, "Development of active lower limb robotic-based orthosis and exoskeleton devices: A systematic review," *Int. J. Soc. Robot*, 1–19, Jun. 2020. DOI: 10.1007/s12369-020-00662-9.
10. S. Mohan, J. K. Mohanta, S. Kurtenbach, J. Paris, B. Corves, and M. Huesing, "Design, development and control of a 2PRP-2PPR planar parallel manipulator for lower limb rehabilitation therapies," *Mech. Mach. Theory*, Vol. 112, pp. 272–94, Jun. 2017.
11. M. Cestari, D. Sanz-Merodio, J. C. Arevalo, and E. Garcia, "ARES, a variable stiffness actuator with embedded force sensor for the ATLAS exoskeleton," *Ind Rob: An Int. J*, Vol. 41, pp. 518–26, Oct. 2014.
12. O. Baser, H. Kizilhan, and E. Kilic, "Biomimetic compliant lower limb exoskeleton (BioComEx) and its experimental evaluation," *J. Braz. Soc. Mech. Sci. & Eng*, Vol. 41, pp. 226, May 2019.
13. S. K. Banala, S. K. Agrawal, S. H. Kim, and J. P. Scholz, "Novel gait adaptation and neuromotor training results using an active leg exoskeleton," *IEEE. ASME. Trans. Mechatron.*, Vol. 15, pp. 216–25, Feb. 2010.
14. R. Riener, L. Lünenburger, I. C. Maier, G. Colombo, and V. Dietz, "Locomotor training in subjects with sensori-motor deficits: an overview of the robotic gait orthosis lokomat," *J. Healthc. Eng.*, Vol. 1, pp. 197–216, Jun. 2010.
15. J. F. Veneman, R. Kruidhof, E. E. Hekman, R. Ekkelenkamp, E. H. Van Asseldonk, and H. Van Der Kooij, "Design and evaluation of the LOPES exoskeleton robot for interactive gait rehabilitation," *IEEE Trans. Neural Syst. Rehabilitation Eng*, Vol. 15, pp. 379–86, Sep. 2007.
16. Y. Long, Z. Du, C. Chen, W. Wang, L. He, X. Mao, G. Xu, G. Zhao, X. Li, and W. Dong, "Development and analysis of an electrically actuated lower extremity assistive exoskeleton," *J. Bionic Eng.*, Vol. 14, pp. 272–83, Jun. 2017.
17. H. T. Tran, H. Cheng, H. Rui, X. Lin, M. K. Duong, and Q. Chen, "Evaluation of a fuzzy-based impedance control strategy on a powered lower exoskeleton," *Int. J. Soc. Robot*, Vol. 8, pp. 103–23, Jan. 2016.
18. M. Vasanthakumar, B. Vinod, J. K. Mohanta, and S. Mohan, "Design and robust motion control of a planar 1P-2P RP hybrid manipulator for lower limb rehabilitation applications," *J. Intell Robot Syst*, Vol. 96, pp. 17–30, Oct. 2019.
19. S. Hussain, S. Q. Xie, and P. K. Jamwal, "Control of a robotic orthosis for gait rehabilitation," *Rob. Auton. Syst.*, Vol. 61, pp. 911–9, Sep. 2013.
20. A. P. P. A. Majeed, Z. Taha, A. F. Z. Abidin, M. A. Zakaria, I. M. Khairuddina, M. A. M. Razman, and Z. Mohamed, "The control of a lower limb exoskeleton for gait rehabilitation: a hybrid active force control approach," *Procedia. Comput. Sci.*, Vol. 105, pp. 183–90, Jan. 2017.
21. Q. T. Dao, and S. I. Yamamoto, "Tracking control of a robotic orthosis for gait rehabilitation: A feedforward-feedback control approach," in *Proc. 10th Biomedical Engineering International Conference (BMEiCON)*, Hokkaido, Japan, 2017, pp. 1–5.
22. Z. Shen, J. Zhou, J. Gao, and R. Song, "Fuzzy logic based PID control of a 3 DOF lower limb rehabilitation robot," in *Proc. IEEE 8th Annual International Conference on CYBER Technology in Automation, Control, and Intelligent Systems (CYBER)*, Tianjin, China, 2018, pp. 818–21.
23. J. Narayan, A. Kalani, and S. K. Dwivedy, "Reference trajectory based Jacobian transpose control of a novel lower limb exoskeleton system for children," in *Proc. IEEE 5th International Conference On Signal Processing, Computing And Control (ISPCC)*, Solan, India, 2019, pp. 102–7.
24. S. K. Banala, S. K. Agrawal, and J. P. Scholz, "Active Leg Exoskeleton (ALEX) for gait rehabilitation of motor-impaired patients," in *Proc. IEEE 10th International Conference On Rehabilitation Robotics*, Noordwijk, Netherlands, 2007, pp. 401–7.
25. D. A. Winter, *Biomechanics and motor control of human movement*. Waterloo: John Wiley & Sons, 2009.
26. T. Malone, T. A. Blackburn, and L. A. Wallace, "Knee rehabilitation," *Phys. Ther.*, Vol. 60, pp. 1602–10, Dec. 1980.
27. Z. Zhang, "Microsoft kinect sensor and its effect," *IEEE Multimedia*, Vol. 19, pp. 4–10, Apr. 2012.
28. C. Elliott, V. Vijayakumar, W. Zink, and R. Hansen, "National instruments LabVIEW: a programming environment for laboratory automation and measurement," *JALA-J Lab Auto*, Vol. 12, pp. 17–24, Feb. 2007.
29. National Instruments, Kinesthesia Toolkit for Microsoft Kinect - University of Leeds. <http://sine.ni.com/nips/cds/view/p/lang/en/nid/210938>, [cited: 02 march 2020].
30. J. Narayan, A. Pardashani, and S. K. Dwivedy, "Comparative gait analysis of healthy young male and female adults using Kinect-Labview setup," in *Proc. IEEE 1st International Conference on Computational Performance Evaluation (ComPE)*, Shillong, India, 2020, pp. 688–93.
31. J. J. Craig, *Introduction to robotics: mechanics and control*. Upper Saddle River, NJ: Pearson Prentice Hall, 2005, p. 150–1.

32. J. Wu, J. Gao, R. Song, R. Li, Y. Li, and L. Jiang, "The design and control of a 3DOF lower limb rehabilitation robot," *Mechatronics. (Oxf)*, Vol. 33, pp. 13–22, [Feb. 2016](#).
33. S. Cong, and Y. Liang, "PID-like neural network nonlinear adaptive control for uncertain multivariable motion control systems," *IEEE Trans. Ind. Electron*, Vol. 56, pp. 3872–9, [Apr. 2009](#).
34. P. J. Gaidhane, M. J. Nigam, A. Kumar, and P. M. Pradhan, "Design of interval type-2 fuzzy pre compensated PID controller applied to two-DOF robotic manipulator with variable payload," *ISA Trans.*, Vol. 89, pp. 169–85, [Jun. 2019](#).
35. G. Goswami, and P. K. Goswami, "ANFIS Supervised PID controlled SAPF for Harmonic current Compensation at nonlinear Loads," *IETE. J. Res.*, 1–12, [Jun. 2020](#). DOI: [10.1080/03772063.2020.1770134](#).
36. J. S. Jang, "ANFIS: adaptive-network-based fuzzy inference system," *IEEE T Syst Man Cy*, Vol. 23, pp. 665–85, [May 1993](#).
37. S. Tripathi, A. Upadhyay, S. Kotyan, and S. Yadav, "Analysis and Comparison of different fuzzy inference systems used in Decision Making for Secondary Users in Cognitive Radio network," *Wirel. Pers. Commun.*, Vol. 104, pp. 1175–208, [Feb. 2019](#).
38. I. Goldhirsch, P. L. Sulem, and S. A. Orszag, "Stability and Lyapunov stability of dynamical systems: A differential approach and a numerical method," *Physica D*, Vol. 27, pp. 311–37, [Aug. 1987](#).
39. J. A. Vargas, W. Pedrycz, and E. M. Hemerly, "Improved learning algorithm for two-layer neural networks for identification of nonlinear systems," *Neurocomputing*, Vol. 329, pp. 86–96, [Feb. 2019](#).
40. M. A. Maghenem, and A. Loria, "Strict Lyapunov functions for time-varying systems with persistency of excitation," *Automatica. (Oxf)*, Vol. 78, pp. 274–9, [Apr. 2017](#).

---

## Authors



**Jyotindra Narayan** received his Bachelor of Technology (B. Tech) in Mechanical Engineering from Uttar Pradesh Technical University, India in 2014. Thereafter, he completed his Master of Engineering (M.E.) from Thapar University, Patiala in 2017 with the specialization of CAD/CAM and robotics, where he worked on the patient side medical manipulators. Now, he is currently a Ph.D. student in Mechanical Engineering Department at Indian Institute of Technology Guwahati (IIT Guwahati), India. His focused research interests are medical assisted robotics, rehabilitation devices for motion assistance and adaptive as well as intelligent control designs in robotics.

**Corresponding author. Email:** [n.jyotindra@gmail.com](mailto:n.jyotindra@gmail.com)



**Santosha Kumar Dwivedy** received the Ph.D. in Mechanical Engineering from Indian Institute of Technology Kharagpur (IIT Kharagpur), India in 2000. He is currently Professor in Department of Mechanical Engineering at Indian Institute of Technology Guwahati (IIT Guwahati). He was also a Visiting Professor at Institute of Engineering and Computational Mechanics, University of Stuttgart, Germany under DAAD-IIT faculty exchange scheme. He has over 180 journal and conference publications with a focus on integrating robotics and dynamics in various fields. His research interests include both industrial and medical robotics, biomechanics, nonlinear vibration and control along with the applications.

**Email:** [dwivedy@iitg.ac.in](mailto:dwivedy@iitg.ac.in)

---